Article

Cell

Chromosomes Progress to Metaphase in Multiple Discrete Steps via Global Compaction/Expansion Cycles

Graphical Abstract

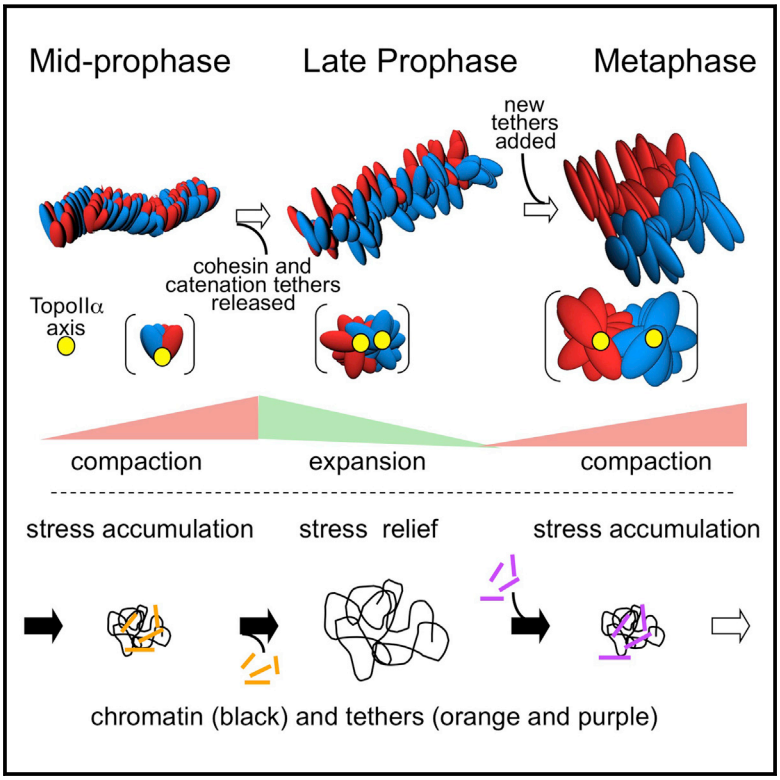

Authors

Zhangyi Liang, Denise Zickler, ..., Kazuhiro Maeshima, Nancy Kleckner

Correspondence

kleckner@fas.harvard.edu

In Brief

Chromosomes undergo cycles of global compaction and expansion, potentially driven by alternating accumulation and release of mechanical stress, as they progress from prophase to metaphase.

Highlights

- Chromosomes progress from prophase to metaphase via three discrete intermediates
- Prophase chromosomes comprise intermingled sister loops along a kinked peripheral axis
- Post-prophase expansion promotes sister-axis splitting and radial-loop disposition
- Compaction/expansion cycles match accumulation/relief of internal chromosome stress

Liang et al., 2015, Cell *161*, 1124–1137
May 21, 2015
http://dx.doi.org/10.1016/j.cell.2015.04.030

CellPress

Cell

Article

Chromosomes Progress to Metaphase in Multiple Discrete Steps via Global Compaction/Expansion Cycles

Zhangyi Liang,[1] Denise Zickler,[3] Mara Prentiss,[2] Frederick S. Chang,[1] Guillaume Witz,[1] Kazuhiro Maeshima,[4] and Nancy Kleckner[1,*]

[1]Department of Molecular and Cellular Biology

[2]Deparment of Physics

Harvard University, Cambridge, MA 02138, USA

[3]Institut de Génétique and Microbiologie, Université Paris-sud, 91405 Orsay Cedex, France

[4]National Institute of Genetics and Graduate University for Advanced Studies (Sokendai), Mishima, Shizuoka 411-8540, Japan

*Correspondence: kleckner@fas.harvard.edu

http://dx.doi.org/10.1016/j.cell.2015.04.030

SUMMARY

Mammalian mitotic chromosome morphogenesis was analyzed by 4D live-cell and snapshot deconvolution fluorescence imaging. Prophase chromosomes, whose organization was previously unknown, are revealed to comprise co-oriented sister linear loop arrays displayed along a single, peripheral, regularly kinked topoisomerase II/cohesin/condensin II axis. Thereafter, rather than smooth, progressive compaction as generally envisioned, progression to metaphase is a discontinuous process involving chromosome expansion as well as compaction. At late prophase, dependent on topoisomerase II and with concomitant cohesin release, chromosomes expand, axes split and straighten, and chromatin loops transit to a radial disposition around now-central axes. Finally, chromosomes globally compact, giving the metaphase state. These patterns are consistent with the hypothesis that the molecular events of chromosome morphogenesis are governed by accumulation and release of chromosome stress, created by chromatin compaction and expansion. Chromosome state could evolve analogously throughout the cell cycle.

INTRODUCTION

Chromosome organization and function reflect diverse molecular inputs coordinated by regulatory circuitry. We wondered whether there might be additional, general principles reflecting the physical or mechanical properties of the chromosomes. We proposed (Kleckner et al., 2004) that chromosomes undergo cyclic global alternation between compact and expanded states that correspond, respectively, to accumulation and release of internal stress. Energy released by progression to the less stressed state would do chromosomal work of diverse types, globally throughout the chromosomes.

This "chromosome stress cycling" would work as follows. When a DNA/chromatin fiber is unconstrained, it will occupy a particular volume that balances maximization of entropy with minimization of interactions among segments (excluded volume). If this fiber is constrained into a too-small volume by inter-fiber tethers, it will be "scrunched" into an unfavorable high-potential energy condition; that is, it will be stressed. If tethers are released, the fiber will tend to straighten out, with accumulated stress released via chromatin expansion.

If such effects occur in the context of chromosomes, they can influence chromosome state. During expansion, different chromatin segments tend to separate from one another, both along a fiber and between/among different linked or confined chromatin units (loops, domains, or whole chromosomes). In effect, different chromatin segments or units will tend to "push one another apart," thus mediating chromosomal changes. Compaction, oppositely, will override these tendencies to permit/promote installation of a new set of constraining tethers. Such effects would lock in the features created by expansion and restore a scrunched, stressed chromatin state, setting the stage for a next round of expansion/stress-promoted changes.

Tethers could comprise any molecular interaction that links two (or more) DNA segments (e.g., cohesin, condensin, CTCF, RNAs, histone-histone contacts) as well as topoisomerase II (TopoII)-mediated catenations between the topologically closed domains created by such links. The free energy decrease that drives expansion-mediated changes would have an important entropic component, reflecting reduced confinement of the DNA/chromatin fiber, but will also involve enthalpic components, e.g., from changes in proteins, RNAs, or DNA state per se.

By this scenario, chromosomes could evolve through the cell cycle by a step-wise process. Periods of expansion-mediated change would alternate with periods of compaction, during which chromosomes would carry out functions enabled by their newly acquired state.

This hypothesis emerged in part from experimental identification of global chromosome expansion/compaction cycles in meiotic prophase chromosomes (Kleckner et al., 2004). These chromosomes are locked into a specific conformation, with chromatin loops linearly arrayed along a structural axis meshwork and sister chromatids closely conjoined in co-oriented

linear loop arrays (Zickler and Kleckner, 1999; Kleckner, 2006; Page and Hawley, 2004). In this condition, chromatin expansion/compaction can be seen cytologically as increased/decreased diffuseness or volume. Expansion and compaction are accompanied by tendencies for increased and decreased separateness of sister chromatids, matching predicted effects of chromatin "pushing" (Kleckner et al., 2004). Meiotic chromosomes also exhibit spatial patterns of the type expected for a stress-mediated process: crossover recombination sites, which are specified during a period of chromosome expansion, tend to be evenly spaced (Kleckner et al., 2004; Zhang et al., 2014a, 2014b).

Recent findings support a role for stress cycling as a general feature of chromosomal programs. In *E.coli*, chromosome length (and thus volume) cyclically increases and decreases. Moreover, increases are correlated with increased sister separation that is licensed by release of programmed inter-sister tethers, implying release of accumulated stress (Fisher et al., 2013). In budding yeast, even spacing of meiotic crossovers requires the catalytic activity of TopoII (Zhang et al., 2014b), whose role is to alleviate mechanical stress resulting from DNA supercoiling and/or catenation/knotting between/within topologically closed domains.

The current study explores the "stress hypothesis" in the context of the mitotic chromosomal program. Chromosomes progress from a diffuse "interphase" state to the compact, well-organized metaphase state and then return to a diffuse state. We examined the period of metaphase chromosome assembly with the notion that phenomena and effects relevant to our hypothesis might be read out directly in cytologically observable morphological changes.

Along metaphase chromosomes, sister chromatids are side-by-side and each comprises a radial array of chromatin loops linked by structural components at their bases (Marsden and Laemmli, 1979; Kleckner et al., 2013; Naumova et al., 2013; Maeshima and Eltsov, 2008). Century-old studies define a discrete preceding stage, "prophase," in which replicated chromosomes comprise long, thin, morphologically single units that are broadly bent into so-called "spiremes," as seen in plants (Kuwada, 1939; Bajer, 1959) and mammals, e.g., human (Ohnuki, 1968) and Indian muntjac (Giménez-Abián et al., 1995). The organization of this prominent intermediate, and thus the nature of its progression to metaphase, is unknown.

Textbook considerations assume that progression from interphase to prophase to metaphase involves smoothly continuous compaction. However, as noted previously (Kleckner et al., 2004), one intriguing live-cell study of giant plant chromosomes suggested that formation of prophase chromosomes is followed by a period of chromosome expansion that includes individualization of sister chromatids (Bajer, 1959), hinting at a possible compaction/expansion stress cycle. We have now explored events of the corresponding period in mammalian systems to define their nature; determine whether they involve expansion as well as compaction; determine whether changes correspond to those expected for stress cycling; and further understand the basis for, and functional implications of, such a process.

We applied four-dimensional (three dimensions over time) epifluorescence deconvolution microscopy to mammalian cells of Indian muntjac (deer), human, and pig. Time-lapse imaging of individual single cells was complemented by snapshot and spread-chromosome analyses.

RESULTS

Prophase to Metaphase in Living Indian Muntjac and HeLa Cells

Living HeLa and Indian muntjac cells were synchronized, released from arrest, and imaged at appropriate times thereafter. Muntjac chromosomes were visualized by Hoechst staining and snapshot analysis (Figures 1A and 1C; Figure S1). HeLa cells expressing histone H2B-GFP were visualized by single-cell time-lapse imaging (Figures 1B and S2, below). Onset of prophase (when DNA/chromatin densities are first visible) to metaphase (when chromosomes are clustered along the spindle mid-plane) comprises ~40 min in both species. The same morphological progression occurs in both cases.

Prophase comprises three stages. (1) *Early prophase*. Chromosomes are fluffy and irregularly shaped and cannot be traced continuously end-to-end (Figures 1A and 1B). (2) *Mid-prophase.* Chromatin coalesces into discrete, morphologically single chromosome units that are broadly but irregularly curved (Figures 1A–1C) and exhibit sharp, discrete bends. These patterns correspond to classical images of prophase chromosomes. (3) *Late prophase*. Chromosomes become noticeably straighter and wider (Figures 1A and 1B). Analogous stages were distinguished previously (Kireeva et al., 2004).

Nuclear envelope breakdown (NEB) defines the end of prophase. During and after NEB, chromosomes continue to become straighter and wider and noticeably shorter (Figure 1A). Sister chromatids become visibly distinct along their lengths only at late metaphase (Figure 1A). Notably, the "iconic X-shape" of textbooks arises only in response to drug-induced metaphase arrest (Nakajima et al., 2007).

Chromosomes Expand during Late Prophase and then Compact

Coalescence of fluffy early prophase chromosomes into discrete mid-prophase chromosomes implies DNA/chromatin compaction. To determine whether compaction continues progressively to metaphase, chromosome volumes were defined from mid-prophase onward. By three criteria, chromosomes expand during late prophase and then compact dramatically after NEB into metaphase.

(1) In individual HeLa histone H2B-GFP nuclei (Figure 2A), the distribution of H2B-GFP intensities provides a readout of chromatin density. This distribution shifts to lower values from mid-prophase to late prophase and then, dramatically, to higher values thereafter (seen for all pixels of all xy planes and for a selected individual plane; Figures 2B, 2C, and S2F–S2I). By implication, chromatin initially expands and then compacts.

(2) The same progression is seen when these nuclei are analyzed directly for chromosome volume by Volocity software, with volume defined as the number of voxels with an intensity above an appropriately defined threshold (Figure 2E).

(3) Living muntjac cells exhibit the same pattern by Volocity volume analysis of 3D snapshots of Hoechst 33342-stained chromosomes (Figures 2D and 2F).

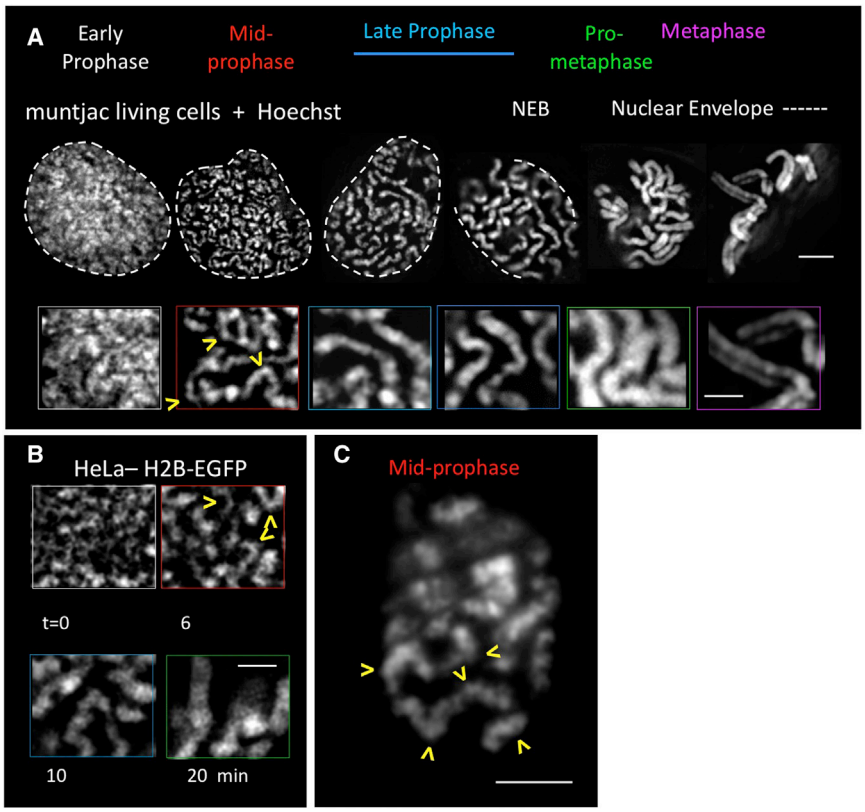

Figure 1. Stages of Mitotic Chromosome Morphogenesis in Living Muntjac and HeLa Cells

Living whole cells were imaged in 3D by epifluorescence microscopy from early prophase to metaphase. Stages illustrated by single-plane images (1× deconvolution).

(A) Snapshots from living muntjac cells stained with Hoechst 33342. Yellow arrowheads indicate chromosome bends specific to mid-prophase.

(B) Selected images from time-lapse analysis of a single HeLa H2B-EGFP cell. Colors as in (A).

(C) Second muntjac mid-prophase nucleus as in (A). Dashed line indicates nuclear envelope.

NEB = nuclear envelope breakdown. Bars: (A) top row and (C) = 5 μm; (A) bottom row and (B) = 2 μm. See also Figure S1.

To evaluate the basis for these volume changes, we defined chromosome widths and contour lengths from mid-prophase onward. For living HeLa histone H2B-GFP and muntjac cells, chromosome widths were defined via traces perpendicular to chromosome paths in single planes of 3D z stacks (Figure 2G). To define chromosome lengths, each nucleus was divided into a top and bottom half, and the signals in each half were projected in the z dimension onto a single xy plane, giving displays of chromosome paths with little overlap (Figure 2J). Chromosome lengths were defined by tracing along the paths and summing results for the two halves. Additionally, to avoid complexities from 3D projection analysis, lengths were also defined for surface-spread muntjac chromosome preparations (Figure 2K).

All measurements indicate that (1) chromosome width increases from mid-prophase to late prophase and then further increases thereafter, more dramatically for muntjac than for HeLa cells (Figures 2H and 2I); and (2) chromosome contour length does not change significantly from mid-prophase to late prophase but decreases progressively thereafter (Figures 2L and 2M). Thus, chromosome expansion during late prophase results from an increase in chromosome width with no change in chromosome length, whereas compaction during prometaphase-to-metaphase results from a further increase in width plus a dramatic decrease in length.

Mid-Prophase Chromosomes Have a "Meiotic-like" Organization but a Kinked Conformation

To understand the organizational basis for alternating chromatin expansion and compaction, we analyzed the morphological nature of prophase and ensuing stages. Mitotic mid-prophase chromosomes closely resemble meiotic prophase chromosomes, appearing as long, thin units comprising closely juxtaposed sister chromatids (Zickler and Kleckner, 1999) and, in Indian muntjac, being nearly identical in length (Giménez-Abián et al., 1995 versus Ma and Shi, 1988). In meiotic chromosomes, sister chromatids are known to be organized into closely conjoined coriented linear arrays of chromatin loops, decorated at their bases by a structural axis that includes TopoII, cohesin(s), and condensin(s) plus meiosis-specific proteins (Kleckner, 2006; Page and Hawley, 2004; Moens and Earnshaw, 1989). We examined mitotic mid-prophase chromosomes for these same features.

TopoIIα

The disposition of TopoIIα was analyzed by indirect immunofluorescence of muntjac and HeLa cells and single-cell time-lapse imaging of pig LLC-Pk cells expressing EGFP-TopoIIα (Tavormina et al., 2002). All approaches give the same picture (Figures 3, 4, S2C, and S2D). At early prophase, TopoIIα signals are diffuse and/or punctate (Figure 3A). By mid-prophase, each chromosome exhibits a single narrow TopoIIα signal extending along its length in an irregular path (Figures 3A and 3B), pointing to presence of a single structural axis. At late prophase, this axis splits, region-by-region, ultimately along the entire chromosome (Figures 3A and 3B). By NEB and into metaphase, each chromosome exhibits a parallel array of TopoIIα signals (Figures 3A and 3B), known to comprise the centrally localized axes of sister chromatids (Maeshima and Laemmli, 2003; Maeshima and Eltsov, 2008).

The mid-prophase TopoIIα axis was further defined by 3D analysis (Figures 4A and 4B). It tends to be located "peripherally" with respect to the chromatin (as in meiotic prophase chromosomes) as seen by 3D reconstructions (Figure 4A), "tube-end views" in muntjac, HeLa, and pig (Figure 4B), and z stack analysis of surface-spread preparations (Figure S3).

Three-dimensional reconstructions reveal two additional features, highlighted by the paths of the centroids of the TopoIIα

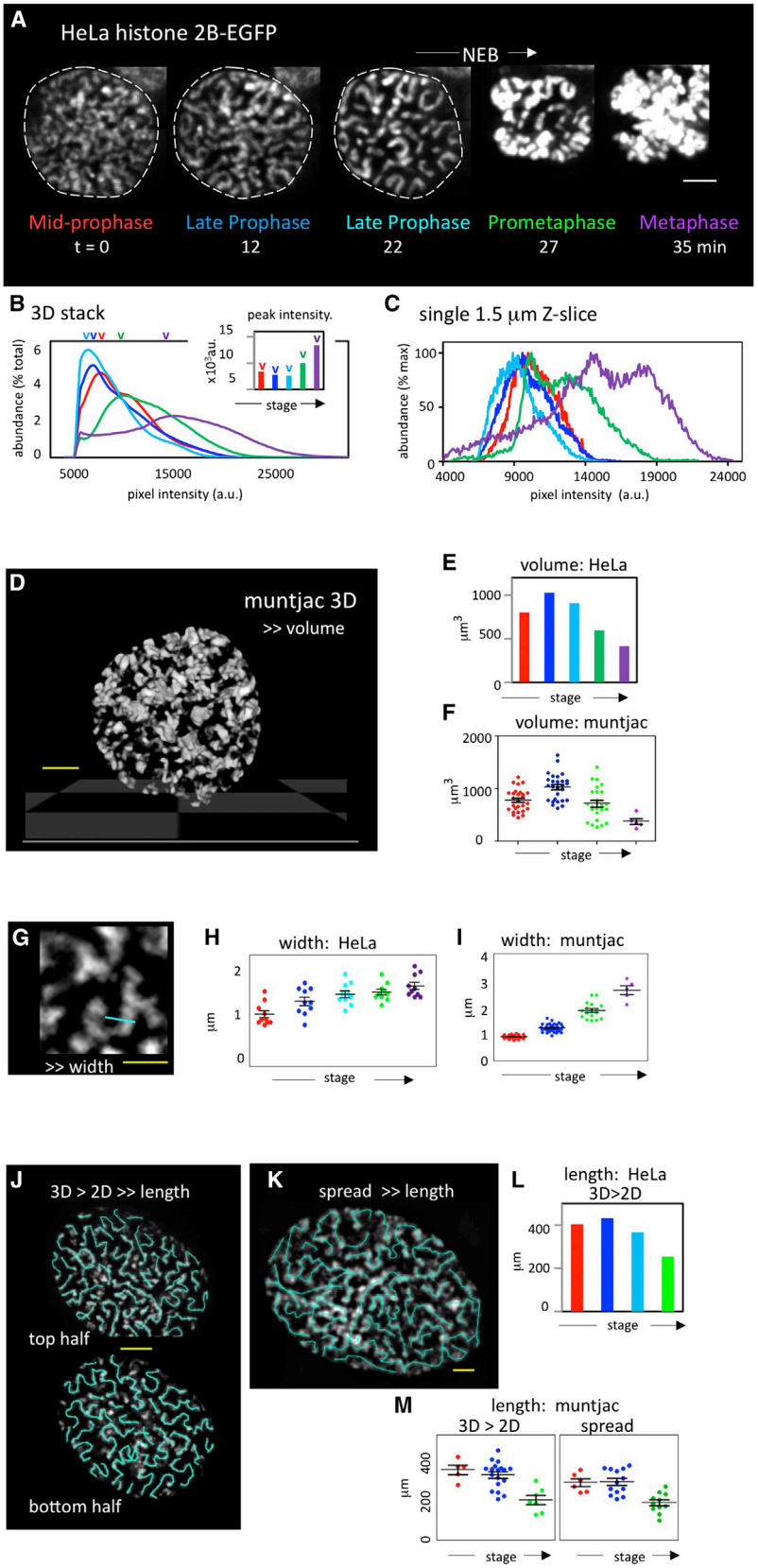

Figure 2. Chromosome Compaction/Expansion Cycles and Changes in Chromosome Width and Length

(A–F) Chromosome compaction/expansion. (A) Three-dimensional single-cell time-lapse imaging of a HeLa histone H2B-GFP cell. Successive stages illustrated by maximum intensity projections of 1.5 µm z slices. (B and C) Distributions of pixel intensities at successive stages for (B) entire 3D stacks plus corresponding maximally abundant pixel intensities (inset) and (C) 1.5 µm z slices shown in (A). From mid-prophase (red), chromatin expands during late prophase (progressive decrease in intensities; dark to light blue); chromatin compacts during prometaphase (green) and metaphase (purple) (progressive increase in intensities). (D) 3D rendering of a living muntjac Mid-prophase nucleus (Hoechst 33342). (E and F) Chromosome volumes of whole nuclei defined by Volocity software as number of voxels above an appropriate intensity threshold for (E) the HeLa histone H2B-GFP nuclei in (A)–(C) and (F) living Hoechst 33342-stained muntjac nuclei at the indicated stages (colored as in A). In both (E) and (F), volumes increase from mid-prophase (red) to late prophase (light to dark blue) and then decrease from prometaphase through metaphase (green and purple).

(G–I) Chromosome widths. (G) Widths defined from traces across chromosomes perpendicular to their lengths in single-plane images (turquoise bar). (H) Widths in the HeLa histone H2B-GFP nuclei of (A)–(C) and (E). (I) Widths for muntjac chromosomes from nuclei analyzed in (F) (stages colored as in A). In both (H) and (I), chromosome width increases progressively from mid-prophase to prometaphase and beyond into metaphase (also Figure 5F below).

(J) Chromosome lengths were analyzed in 3D z stacks by projecting the top and bottom halves of each nucleus onto a single xy plane, tracing of chromosome contours, and summing the lengths in the two halves.

(K) Contour lengths traced in spread muntjac chromosomes.

(L) Lengths determined as in (J) for 3D stacks of the HeLa histone H2B-GFP nuclei in (A)–(C), (E), and (H).

(M) Lengths for the muntjac nuclei analyzed in 3D in (F) and (I) (left) and in spread preparations as in (K) (right).

Bars = 5 µm (A, D, J, and K); 2 µm (G). See also Figure S2.

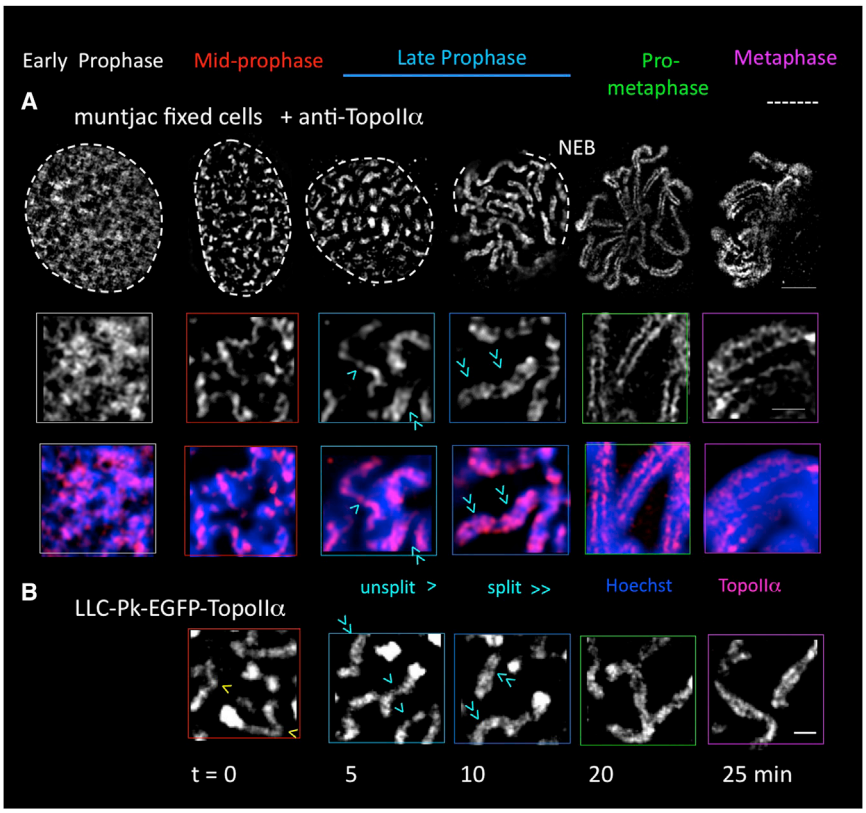

Figure 3. Mid-Prophase Chromosomes Exhibit a Single TopoIIα Axis

(A) Three-dimensional epifluorescence images of fixed cells stained with DAPI and anti-TopoIIα. Single-plane images are from snapshots at the indicated stages (1× deconvolution). Top and middle rows: TopoIIα. Bottom row: TopoIIα overlaid on DAPI. TopoIIα signal is diffuse/disorganized at early prophase (left), forms a single narrow linear signal along mid-prophase chromosomes (second from left), and splits region-by-region at late prophase (turquoise arrows). Prometaphase and metaphase chromosomes (right) exhibit two parallel TopoIIα signals corresponding to sister chromatids. Dashed line indicates nuclear envelope. NEB = nuclear envelope breakdown. Bars: top row = 5 μm; middle and bottom rows = 2 μm. (B) Three-dimensional time-lapse imaging of a pig LLC-Pk EGFP-TopoIIα cell reveals the same progression of TopoIIα signals as for muntjac in (A) (single-plane images shown). Bar = 1 μm.

and DNA signals (e.g., for muntjac chromosomes, Figure 4A). (1) The TopoIIα axis meanders around the chromatin periphery. Nonetheless, topologically, this axis does not wind around the chromosome in a helical path; rather, it lies paranemically along one face of the chromatin, in accord with arrangement of the chromatin along a single peripheral axis (Figure 4G, bottom). (2) The path of the axis is kinked in three dimensions. Kinks can be more or less severe (Figure 4A, examples 1 and 2) as two discrete morphological categories (Figure S3E). Interestingly, kinks occur at relatively regular intervals of 0.7 ± 0.2 μm (STD). Dramatic bends also occur, coordinately for TopoIIα and the whole chromosome (Figure 4A) corresponding to bends seen by chromosome staining alone (Figures 1A–1C). Kinked TopoIIα axes occur analogously in living LLC-Pk EGFP-TopoIIα cells (Figure 3B).

Cohesin and Condensin II

Cohesin and condensin II are known to localize to mitotic prophase chromosomes, but sub-chromosomal localization is undefined (Ono et al., 2004; Hirota et al., 2004). We analyzed the localization of Rad21, the kleisin subunit of mammalian cohesin, and hCAP-H2, a component unique to mammalian condensin II, using fixation procedures where strongly bound molecules are preferentially retained ("pre-extraction"; Experimental Procedures). Both molecules occur, with TopoIIα, along the single peripheral mid-prophase axis, as seen in 3D and/or spread-chromosome images (Figures 4C–4E).

Cohesin is known to be lost in bulk from chromosomes during mitotic prophase (Peters and Nishiyama, 2012). We now find that cohesin is released from mid-prophase axes specifically at late prophase (Figure 4D, bottom). In contrast, condensin II remains prominently along prometaphase/metaphase axes (Maeshima and Laemmli, 2003; Ono et al., 2004).

Regularly Arrayed Chromatin (Loops)

Chromatin-loop organization of mitotic mid-prophase chromosomes was probed by a spreading procedure, developed for meiotic chromosomes, that unfolds chromatin loops while maintaining axis integrity, thus revealing regular arrays of loops along linear axes (Møens and Pearlman, 1988). Mitotic mid-prophase chromosomes exhibit the same structure as their meiotic counterparts: a regular chromatin array (presumptively in loops) along a single continuous TopoIIα axis that extends along the entire lengths of the chromosomes, as seen for both muntjac (Figure 4F) and HeLa (Figure S4). In certain regions, dual units occur, consistent with a regular side-by-side sister relationship (Figure 4F, arrow). Later, by prometaphase, chromosomes exhibit regular chromatin arrays along well-separated parallel sister axes, as expected (Figure S4).

Interestingly, for mid-prophase chromosomes, unfolding of loops during spreading is accompanied by two other effects. First, sister loops become splayed out more or less on either side of the axis, despite their original co-oriented relationship defined in 3D. Second, the kinked structure seen in 3D whole-cell images is lost; instead, TopoIIα axes are smoothly continuous along the entire lengths of the chromosomes (Figure 4F, insert). Both effects are explained by loss of linkages between and along chromatids during sample preparation, predicted to alleviate stress (Discussion).

Sister-Chromatid Chromatin Units Individualize during Late Prophase

TopoIIα axes split during late prophase and remain split thereafter (Figure 3A). Thus, sisters might individualize during late prophase, even though visually distinct units are not apparent until

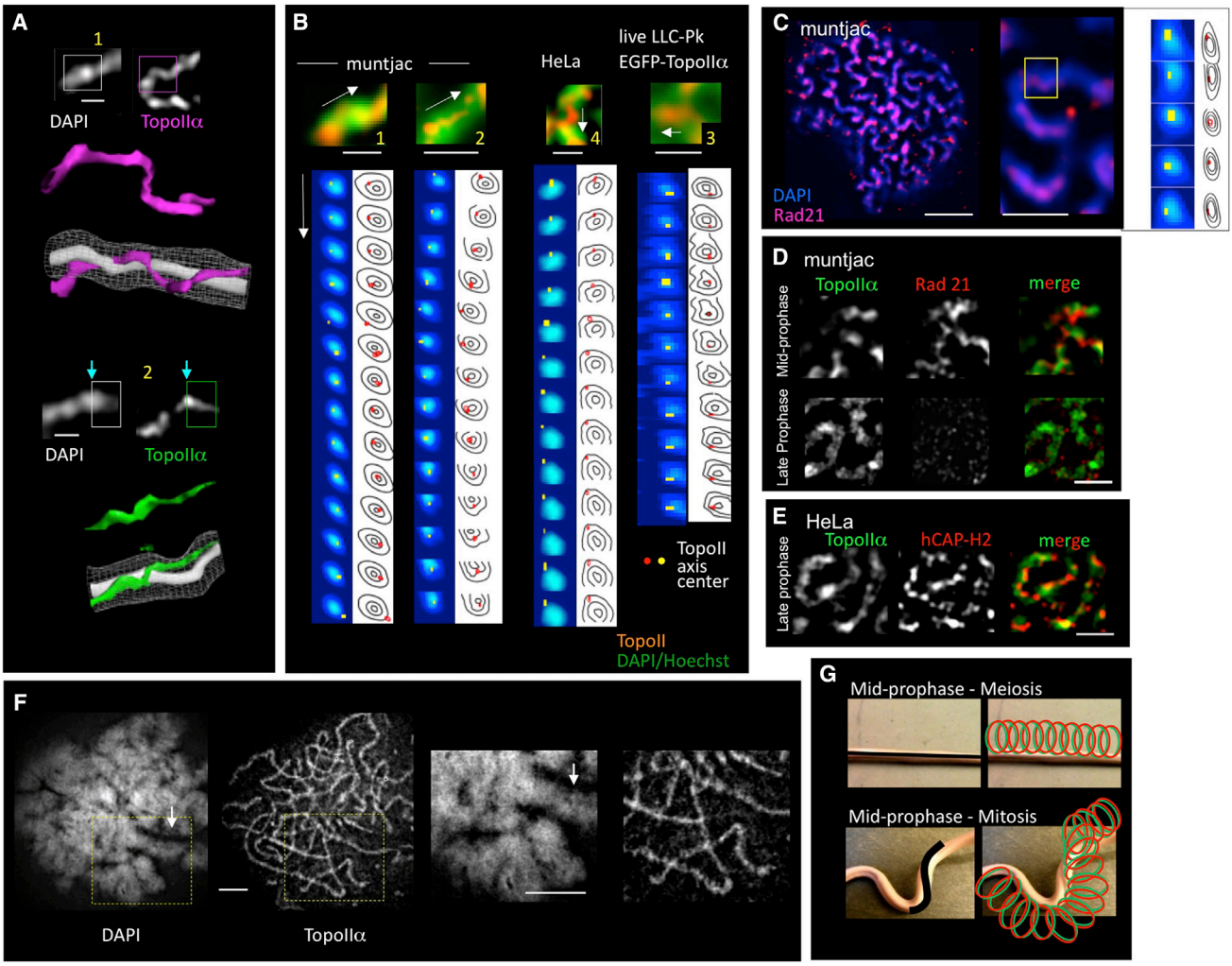

Figure 4. A Regular Array of Loops along a Single Kinked Peripherally Localized Axis Containing TopoIIα, Cohesin, and Condensin at Mid-Prophase

(A) Two muntjac mid-prophase chromosome segments stained with DAPI and anti-TopoIIα (top) are reconstructed as 3D images in PyMOL (bottom). A kinked TopoIIα axis (pink and green) lies peripherally to and paranemically along one face of the chromatin. Segments 1 and 2 illustrate more-kinky and less-kinky paths. The TopoIIα signal (≥95% of maximum pixel intensity) is shown alone; accompanied by an envelope (gray net) representing nearly total chromatin signal (≥60% of maximum pixel intensity); and with the envelope plus the highest density chromatin signal (≥95% of maximum pixel intensity). Turquoise arrows indicate a major bend observed in DNA and TopoIIα paths. Bars = 1 μm.

(B) "Tube-end views" of muntjac, HeLa, and pig chromosome segments (arrows; Supplemental Experimental Procedures). For each cross-section, left and right columns show, respectively, position of the TopoIIα center (maximum intensity pixel) relative to a heatmap of DNA or DNA contours at 95%, 80%, and 50%–60% intensity of the brightest pixel. The TopoIIα signal wanders from one side of the DNA signal to the other (see also A). Examples 1 and 2: muntjac segments as in (A). Examples 3 and 4: segments from pig and HeLa cells (DNA stained with Hoechst and DAPI, respectively). Bars = 1 μm.

(C) Immunostaining of muntjac chromosomes for cohesin Rad21 reveals a peripheral axial signal analogous to that seen for TopoIIα (above). Bars = 5 μm (left) and 2 μm (middle). Right: "tube-end views" as in (B).

(D) Spread muntjac chromosomes double-stained for TopoIIα and Rad21. At mid-prophase, Rad21 localizes along the TopoIIα axis, with differential abundance of the two molecules at different positions (top). At late prophase, Rad21 is lost while TopoIIα remains (bottom). Bar = 2 μm.

(E) HeLa cell double-stained for TopoIIα and condensin II's hCAP-H2. Condensin II localizes along the TopoIIα axis, with different abundancies of the two components at different positions. Bar = 2 μm.

(F) A suitably spread muntjac mid-prophase nucleus shows even arrays of chromatin (presumptively loops) along continuous TopoIIα axes. Arrow indicates region of duality potentially reflecting split sister units (enlarged portion at right). Bar = 5 μm.

(G) Cartoon of meiotic versus mitotic mid-prophase chromosomes. Chromatin loops (red, green) are in a topologically linear array along a single axis (black), which is straight in meiosis (top) or contorted/kinked in mitosis (bottom).

See also Figures S3 and S4.

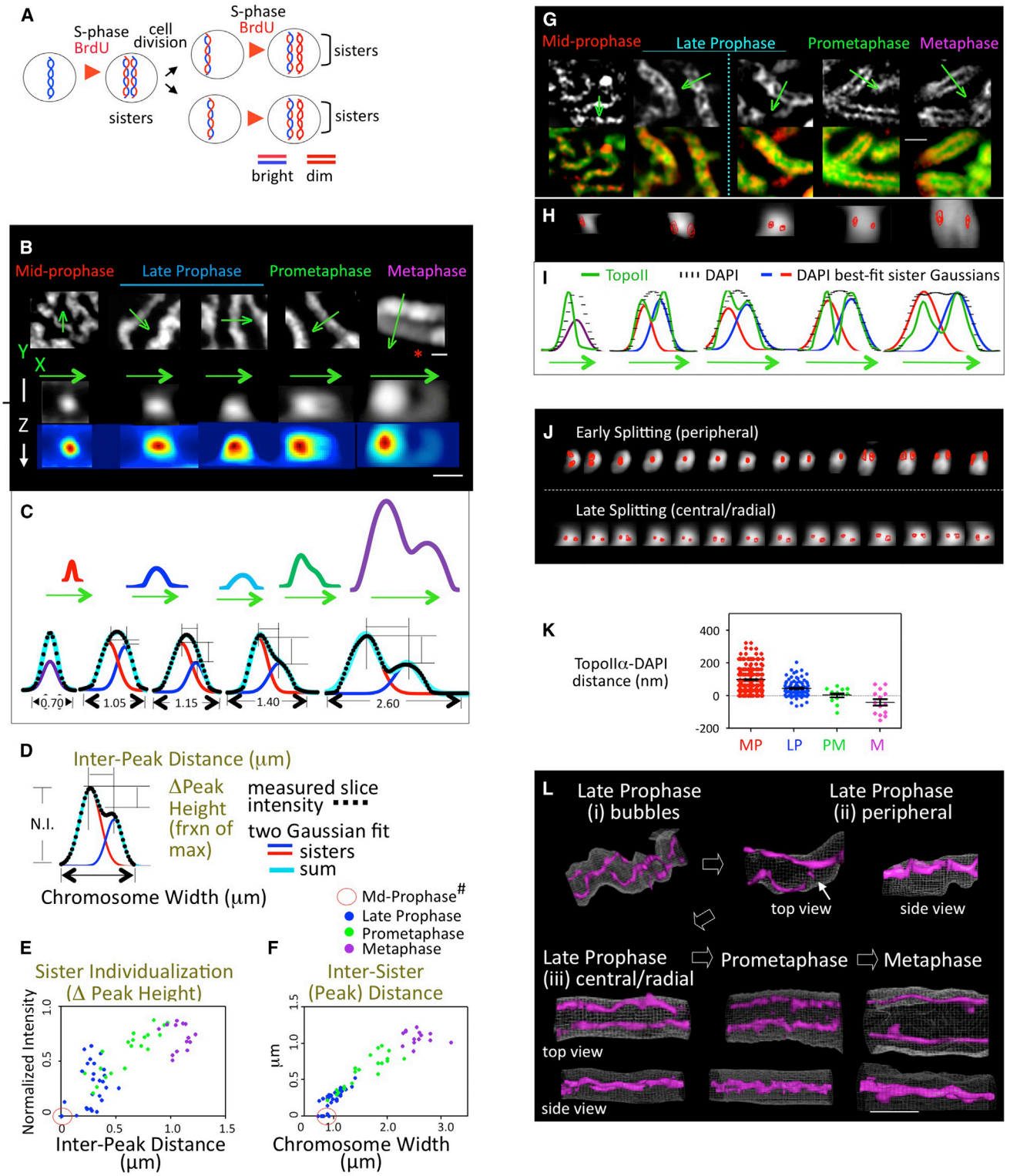

Figure 5. Sister Individualization and Radial Chromatin Disposition Emerge at Late Prophase

(A–F) Sister-chromatid chromatin individualizes during late prophase. (A) Basis for differential BrdU labeling of sister chromatids. (B) Three-dimensional imaging of BrdU-labeled muntjac chromosomes. (Top) Single-plane images representative of successive stages. Red asterisk (right) marks a sister-chromatid exchange. (Bottom) Cross-sections at the positions indicated by arrows at top. (Left to Right) Symmetrical single unit at mid-prophase transits to distinct side-by-side sister units at metaphase. Bars = 1 μm. (C) Top: DAPI intensity profiles along the cross-sections indicated in (B), top. Bottom: DAPI intensity profiles (black dots) were fit

(legend continued on next page)

metaphase (Figure 1A). We therefore defined the timing of sister individualization directly, by differential labeling of sister DNAs.

In chromosomes exposed to two rounds of BrdU incorporation, sisters are labeled on either one or both strands of their DNA duplexes, respectively (Figure 5A). Because BrdU quenches DNA staining by Hoechst 33342, the two sister DNAs give brighter and dimmer Hoechst signals (Figure 5A). This difference is dramatic at metaphase in single-plane images and 3D cross-sections (Figure 5B).

In striking contrast, at mid-prophase, there is no discernible differentiation of sister signals, in single-plane images or in 3D cross-sections, which show a single symmetrical signal (Figure 5B). The same is true in mouse NIH 3T3 chromosomes analyzed by a different method (Figure S5). Thus, to the level of resolution of this analysis, sister DNAs in mid-prophase chromosomes are "well-intermingled."

We next analyzed sister relationships quantitatively from mid-prophase to metaphase. Traces were made perpendicular to chromosome paths in single-plane images (Figures 5B and 5C). Because chromosomes intrinsically comprise two sister DNAs of different staining intensities, the intensity profile of each trace was fit to a pair of Gaussian distributions (Figure 6C). R^2 analysis demonstrates that this is a reliable tool for quantifying the heights and widths of DAPI/BrdU signals (Figure S6E).

Best-fit Gaussian distributions provide two parameters that reflect sister relationships (Figure 5D). "Δ peak height" defines the extent to which sisters are individualized: the two Gaussians will be of different heights according to the different Hoechst intensities of the sisters. "Inter-peak distance" reflects spatial separation of sisters: the two Gaussians will be separated to a greater or lesser extent according to the distance between the two sister density centers.

Mid-prophase chromosomes exhibit no evidence of sister individualization or sister separation. All traces are best fit by a single Gaussian distribution, with presumptive "Δ peak heights" and apparent "inter-peak distances" of zero in all cases (n = 18; Figures 5E and 5F).

Two striking effects emerge at later stages. Δ peak height increases dramatically during late prophase, with only a small increase thereafter (Figure 5E). Thus, sister individualization occurs specifically during this stage, in temporal correlation with loss of cohesin (above). In contrast, inter-peak distance increases progressively from mid-prophase to metaphase, in direct proportion to progressively increasing chromosome width (Figure 5F). Importantly, if chromosomes are stained for DNA without BrdU differential labeling, inter-peak distance (sister separation) again increases progressively in correlation with increased chromosome width but with no difference in sister peak heights at any stage, as expected (Figure S6).

In summary, sister-chromatid chromatin units are well-intermingled at mid-prophase. They individualize during late prophase, with a concomitant initial increase in the distance between sister density centers (sister separation). At prometaphase-through-metaphase, chromosomes with well-individualized sisters become shorter and fatter, with a concomitant further increase in separation of sister-chromatid density centers and a minor further increase in individualization.

Sister Individualization Is Accompanied by Longitudinal Reorganization

At mid-prophase, intermingled sister chromatin occurs peripherally to a single TopoIIα/cohesin/condensin II axis (above). By metaphase, TopoIIα/condensin I/II axes occur centrally within well-individualized sister units (Maeshima and Laemmli, 2003;

to a pair of Gaussians corresponding to sister DNA units (red and blue; summed in turquoise). Curves are normalized such that the maximum peak height = 1; peak widths not normalized. (D) Two-Gaussian best-fit analysis (C, bottom) yields two parameters that define sister relationships (text). (1) "Δ Peak Height" indicates sister individualization. Peak heights for each trace are normalized to a value of one for the highest of the two peaks ("normalized intensity" = "N.I."), with Δ peak height expressed as a fraction of that value. (2) "Inter-Peak Distance" defines sister-chromatid separation. Chromosome widths are defined from traces across chromosomes as in Figures 2G–2I. (E) Mid-prophase chromosomes are fit by a single Gaussian, represented as Δ peak height = zero. Δ peak height increases during late prophase and remains essentially constant thereafter, indicating that sister individualization occurs during late prophase (colors in F). (F) Inter-sister (peak) distance is zero at mid-prophase (circle), then increases progressively, in concert with increased chromosome width, from late prophase through metaphase. Increased width at late prophase reflects sister individualization (E) and thereafter reflects increased center-to-center distance due to increased width of individualized sister units. Deviation for very widest chromosomes reflects a metaphase/anaphase transition stage.

(G–L) Sister chromatin, intermingled and peripheral to a single TopoIIα axis at mid-prophase, becomes radially localized around split TopoIIα axes concomitant with individualization during late prophase. (G) Two-dimensional single-plane images of muntjac chromosomes stained with TopoIIα (top) and merged (red) with DAPI signals (green) (bottom). Bar = 2 μm. (H) Three-dimensional cross-sections of the chromosomes at positions indicated by green arrows in (G), top. (I) Intensity profiles for traces across chromosomes in single planes along green arrows in (G), top) for TopoIIα (green) and DAPI (black). The highest TopoIIα peak and the maximum DAPI intensity were normalized to 1. DAPI profiles were fit by a pair of Gaussians (red and blue) corresponding to two sister units as in (D) and Figure S6. (J) Tube-end views along two late prophase chromosome segments (staining as in G). (Top) Early axis splitting. Split, peripheral axis signals flank an unsplit signal with rotation of the split signal. (Bottom) Segment with complete splitting and sister axis signals located internally to the chromatin. (K) Relative positions of TopoIIα axis peak(s) (Panel I, green) and the peak(s) of Gaussian(s) representing chromosome unit(s) (Panel I, red and blue) at indicated stages. Each mid-prophase case comprises a single peak of each type (DAPI and TopoIIα). At later stages, for each case, the distance between the two Gaussian peaks was subtracted from the distance between the two TopoIIα peaks, and the difference divided by two. Values above zero imply localization of the TopoIIα signals outside of the two Gaussian signals (a peripheral axis/chromosome relationship), whereas values around zero correspond to overlap of the two types of signals (central axes and radially distributed chromatin). At late metaphase (largest widths), below-zero values represent a real tendency for the TopoIIα signals to be closer together than the centers of their sister units at the metaphase/anaphase transition stage seen also in (F). (L) Three-dimensional PyMOL reconstructions of representative segments from muntjac chromosomes at indicated stages. During late prophase: (i) axis split initially as bubbles; (ii) longer split regions are peripheral (arrow indicates junction between split and unsplit regions); and finally, (iii) split regions are located centrally within the chromatin. Thereafter, sister axes further separate as chromosomes widen. (Bottom row) Top and side views show that, at the end of late prophase through metaphase, sisters lie side-by-side with axes centrally located within each sister-chromatid chromatin. TopoIIα signal is ≥ 95% of maximum pixel intensity; DAPI signal is ≥ 60% of maximum pixel intensity. Bar = 1 μm.

See also Figures S5 and S6.

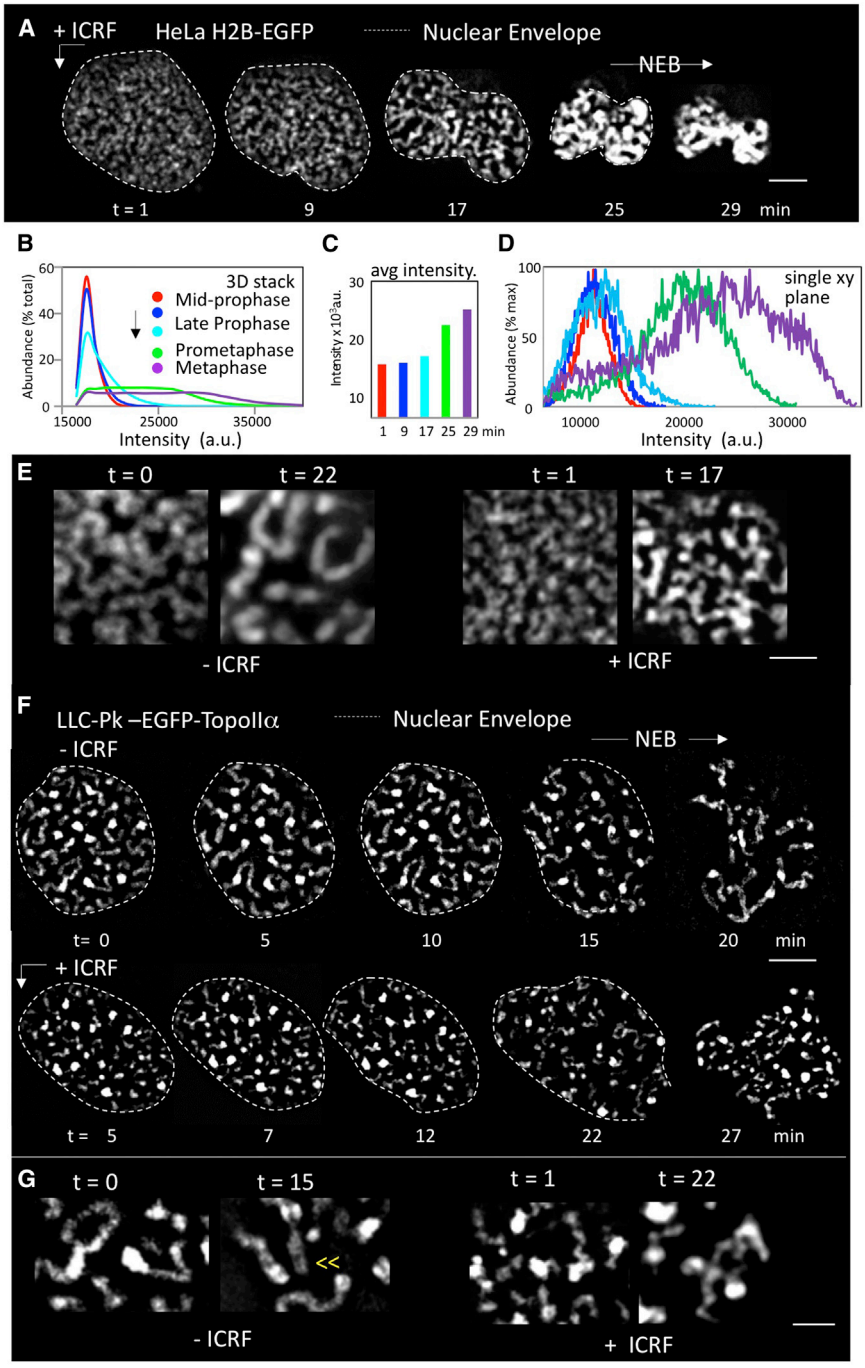

Figure 6. TopoII Activity Is Required for Progression from Mid- to Late Prophase

(A) Three-dimensional time-lapse imaging of a HeLa H2B-GFP cell at mid-prophase identified within a minute after ICRF-193 addition, illustrated by maximum projections of 1.5 μm z slices (compare with Figure 2A for untreated cells). Bar = 5 μm.

(B–D) Distribution of pixel intensities for the nucleus in (A). (B) For each entire 3D stack. (C) Maximum intensities from distributions in (B). (D) For the thick slices in (A). Compare results in (B)–(D) with results for untreated cells in Figures 2B and 2C.

(E) Enlarged portions of single-plane images from untreated cells (left) and treated cells (right) illustrate absence of morphological progression in treated cells. Bar = 2 μm.

(F) Three-dimensional time-lapse imaging of Pig EGFP-TopoIIα cells in the absence (top) or presence (bottom) of ICRF-193 added at mid-prophase as in (A). Bar = 5 μm.

(G) Enlarged images as in (E). (Left) Without ICRF-193, TopoIIα signals are single at mid-prophase and split during late prophase (left; double arrowheads at t = 15 min indicate split region). (Right) In contrast, in the presence of ICRF-193, TopoIIα signals remain unchanged from mid-prophase to a time corresponding to late prophase in untreated cells (right). Bar = 2 μm.

See also Figure S7.

Maeshima and Eltsov, 2008; recapitulated for TopoIIα in Figures 3 and 4, below). We now find that the switch from peripheral to radial chromatin/axis state occurs during late prophase, thus concomitant with sister individualization, and is accompanied by loss of the kinked mid-prophase axis conformation.

For muntjac chromosomes co-stained for DNA and TopoIIα, progression from peripheral to central axis disposition (and thus peripheral to radial DNA disposition) is directly apparent in cross-sectional images (Figures 5H and 5J). At mid-prophase, a single axis occurs at the chromosome periphery (Figure 5H). At the onset of splitting, split TopoIIα axes often occur side-by-side at the periphery of the chromatin (Figure 5H), as in regions that still exhibit both split and unsplit axes (Figure 5J). However, by the end of late prophase, separated sister TopoIIα axis centroids occur well within the chromatin, as also seen at prometaphase and metaphase (Figures 5H and 5J).

Quantitative analysis confirms this progression. TopoIIα and DAPI DNA signals were defined along traces at particular positions along the chromosomes in mid-plane images (Figures 5G and 5I). Sister DNA intensity profiles were defined by two-Gaussian-fit analysis as above (Figures 5D and S6). The position(s) of the peaks for TopoIIα (Figure 5I) and sister units (Figure 5I) were then compared. At mid-prophase, the TopoIIα axis peak is offset from the single DAPI peak, matching peripheral localization of the axis relative to the DNA/chromatin (Figures 4A, 4B, and 5G–5I). In late prophase nuclei, this tendency is markedly reduced as shown by a decreased distance between the two signals, implying ongoing transit from peripheral to central/radial disposition (e.g., Figures 5G–5I and 5K). By prometaphase and into metaphase, DAPI and TopoIIα signal

peaks are very close together, implying fully developed central/radial disposition.

Three-dimensional reconstructions also illustrate this progression (Figure 5L). During late prophase, sister axes initially split in short "bubble" regions, which transit to fully separated but peripherally located axes, and then to axes located centrally within the chromatin, which is radially disposed around each axis. Sister axes then become further separated during prometaphase and metaphase. In accord with radial disposition of chromatin around side-by-side sister axes, at the end of late prophase, and later stages, chromosomes are wider in the dimension in which axes lie side-by-side and narrower in the perpendicular dimension, where axes are aligned and centrally located (Figures 5H and 5L). Three-dimensional reconstructions further show that late-prophase split chromosome axes have lost their bent/kinky mid-prophase conformations (Figures 4A versus 5L), and chromosomes become straighter overall (Figures 1A and 5L).

In summary, late prophase is a major transition stage involving multiple concomitant changes. Axes split and become straighter. Sister-chromatid chromatin units individualize, and their center-to-center distance begins to increase. Sister chromatin units reorganize from a peripheral location relative to a single unsplit axis to a radial disposition around split axes, which become centrally located within their respective sister units. Chromosomes overall become wider and straighter, but their end-to-end contour lengths do not change, with the overall effect being an increase in volume. In essence, the new longitudinal organization seen at metaphase has been established, prior to its reinforcement by global compaction.

Progression out of Mid-Prophase to Late Prophase Requires TopoII Activity

During mitosis, inhibition of TopoII catalytic activity causes defective chromosome morphogenesis, including a tendency for accumulation in a prophase-like state (e.g., Giménez-Abián et al., 1995). However, the time(s) at which inhibition exerts such effect(s) has/have not been precisely staged. Moreover, it is unclear whether/which effects are a direct consequence of TopoII inhibition and which are downstream regulatory effects (e.g., the "G2 decatenation checkpoint"; Deming et al., 2001).

To circumvent these limitations, we added an appropriate TopoII inhibitor (ICRF-193; Giménez-Abián et al., 1995) to a synchronized culture, immediately identified a cell at mid-prophase, and monitored the status of that same individual cell over time thereafter. This protocol was applied to both HeLa histone H2B-GFP cells (Figures 6A–6E) and pig LLC-Pk cells expressing EGFP-TopoIIα (Figures 6F and 6G) to monitor chromatin and TopoIIα axis states, respectively.

Timed ICRF-193 addition arrests chromosomes in their mid-prophase state with respect to both features. Arrest persists for a period of time comparable to that normally required for progression through late prophase (~20 min). NEB and post-NEB chromosome compaction then occur on schedule. Thus, during what should be late prophase, chromosomes do not become wider or straighter (Figure 6E); average chromosome density (and thus chromosome volume) does not change (Figures 6B–6D); and chromosome axes remain single without any discernible change in morphology or path (Figures 6F, 6G, and S7C). However, NEB occurs at the expected time (Figures 6A and 6F; confirmation by lamin staining in Figure S7). Concomitantly, chromatin density increases, implying global compaction, exactly as in untreated cells (Figures 6B–6D).

The likely role of TopoIIα during late prophase is to remove constraining inter-links between protein-enforced topologically closed domains (e.g., but not limited to, chromatin loops). By implication, such interlinks are a prominent feature of mid-prophase chromosomes and must be removed throughout the chromosomes to permit the multiple changes characteristic of late prophase.

DISCUSSION

The presented results reveal the underlying organization of mitotic prophase chromosomes and define the pathway by which these chromosomes progress to metaphase. An unexpectedly complex pathway emerges, characterized by multiple discrete steps and, most notably, chromosome expansion as well as chromosome compaction. The observed patterns closely match those predicted for morphogenesis by the proposed hypothesis of "chromosome stress cycling." We propose that such cycles govern the evolution of chromosomes at all stages of the cell cycle, with accompanying unique characteristic advantages.

We show that prophase chromosomes comprise linear arrays of well-intermingled sister-chromatid loops that emanate from a single peripherally localized structural axis (Figure 7A). This axis includes TopoIIα, cohesion, and condensin II. Hints from spread preparations suggest that each chromatid is organized into its own single linear loop array. Thus, sister loops are likely well-formed but inter-digitated along the chromosome length (as illustrated). Additionally, prophase chromosomes are prominently kinked. Interestingly, shapes reminiscent of those observed here at mid-prophase have been seen for unreplicated G1 chromosomes if cohesin release is blocked (Tedeschi et al., 2013), in accord with a central role for cohesin in creating and maintaining the mid-prophase state.

None of the above features was previously suspected for mitotic prophase chromosomes. However, this organization turns out to be closely analogous to that previously described for meiotic prophase chromosomes, providing satisfying unity between the two programs. The only significant difference is that meiotic chromosome axes are very straight, likely because the axes of homologs (each a sister pair) must be directly linked all along their lengths, e.g., via the synaptonemal complex (Zickler and Kleckner, 1999; Page and Hawley, 2004).

We also show that prophase chromosomes progress to metaphase in two steps (Figure 7A). At late prophase, a basic reorganization occurs. Sisters individualize, axes split, and the chromatin of each sister chromatid reorganizes into a radial disposition around its now-central axis. We infer that chromatin loops have changed from a linear "shoulder-to-shoulder" disposition along their conjoined mid-prophase axis to a radial-loop configuration around each individual chromatid axis. However, chromosome contour length does not change while chromosome volume increases. Then, after NEB, chromosomes

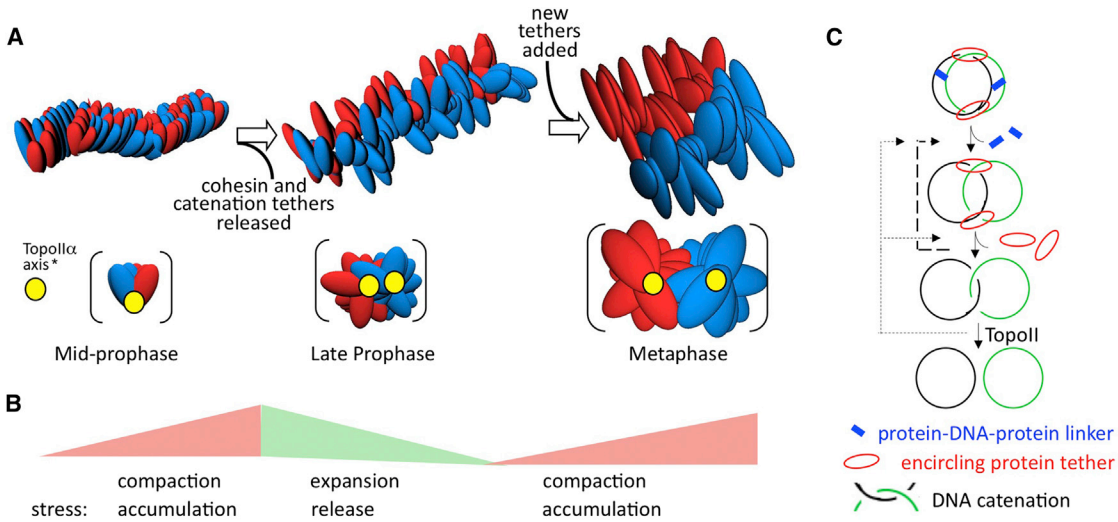

Figure 7. Chromosome Morphogenesis and Expansion/Compaction Stress Cycling

(A) Chromosomes progress from prophase to metaphase via three discrete intermediates. (Left) Mid-prophase chromosomes comprise co-oriented sister linear loop arrays (red and blue) organized along a single peripheral TopoIIα/cohesin/condensin II axis (yellow). (Middle) At late prophase, sister axes split, and the loops of each sister become radially disposed around its respective axis, which has lost cohesin (*). This progression requires release of cohesin and of TopoII-senstive linkages, presumptively catenations. (Right) At metaphase, chromosomes retain the organization established at late prophase but have become shorter and fatter and have acquired new tethers (*).

(B) During the stages in (A), chromosomes alternate between compact and expanded states, interpreted as comprising higher and lower potential energy (more and less stressed) states (pink and green, respectively).

(C) Release of chromosome expansion stress will involve release of different types of constraining linkages, potentially in an autocatalytic process where some release tether(s) increase stress on remaining tethers, promoting their release (etc.).

become shorter and wider, implying that the new organizational state is locked in by dramatic global compaction. This progression could not have been anticipated. Also, chromosomes do not evolve from G2 to metaphase by smooth, progressive compaction, as previously assumed. We find that the actual pathway is discontinuous and involves chromosome expansion as well as chromosome compaction. Together these findings provide a new framework for further defining the roles in chromosome morphogenesis of familiar and newly identified molecules.

Morphogenesis by Compaction/Expansion Stress Cycles?

The "chromosome stress hypothesis" (Introduction) envisions alternation between two distinct states: compact states where chromatin is constrained by programmed inter-segment tethers into a more stressed conformation, and expanded states, where inter-segment tethers are released (Figure 7C) with concomitant relief of stress. Chromatin expansion drives morphological changes because different chromatin segments or units (e.g., loops) tend to push one another apart. Such changes are then locked in by the following compaction stage, concomitantly giving the conformation needed for the next round of expansion-mediated stress-promoted changes. The sequence of events described above matches these and other predictions of the stress hypothesis, as follows.

Chromosomes alternate between compact and expanded conditions: expanded at early prophase; compact at mid-prophase; expanded at late prophase; and compact at prometaphase/metaphase (Figures 7A and 7B). Moreover, these changes involve installation and release of tethers. Topological linkages are prominent at mid-prophase and must be released for progression to late prophase as seen by the effects of TopoII inhibition. Similarly, cohesin, which links pairs of DNAs, is prominent within mid-prophase chromosomes and is released at late prophase (above); moreover, inhibition of this release causes chromosomes to accumulate in a "rod-like state" (Losada et al., 2002) (now presumptively mid-prophase). New tethers are then installed for prometaphase/metaphase compaction (Figure 7A; Kawamura et al., 2010).

During expansion periods, chromosome state changes; during compaction those changes are locked in. Late prophase expansion creates the state seen upon compaction at prometaphase/metaphase. Analogously, early prophase expansion presumably creates the state locked in by compaction into mid-prophase.

Importantly, morphological changes of late prophase directly match those predicted for a stress-promoted transition driven by relief of "chromatin expansion stress," as manifested in both chromatin-loop disposition and axial conformation (Figure 7A).

- At mid-prophase, chromosomes are constrained by linkages between chromatin loops both along and between sisters, giving the "shoulder-to-shoulder" array of inter-mingled sister loops. During late prophase, upon release of these linkages, chromosomes undergo the changes expected if chromatin loops are "pushing" one another into the lowest density state (and thus the lowest energy state) allowed by loop/axis organization. Sister loops push one another apart, provoking axis splitting and sister

individualization, and adjacent loops along each axis push one another into a radial array where they are much less constrained than in the mid-prophase state.

● In the compact mid-prophase state, TopoIIα axes are prominently kinked and whole-chromosome paths exhibit prominent bends. This contorted conformation suggests that the chromosomes are under macroscopic internal stress. Such kinks and bends are expected if adjacent chromatin loops, constrained into their one-dimensional arrays, are trying to "push each other apart" longitudinally along the chromosome but are prevented from doing so by the constraining axis (Kleckner et al., 2004). In the expanded late prophase state, the now-split axes are straight rather than kinked, implying that internal stress has been alleviated. This is the predicted consequence of sister individualization, which halves the number of loops per axis length, plus acquisition of radial-loop configuration, both of which reduce longitudinal loop confinement. Similar effects explain loss of axis kinking in spread mid-prophase chromosomes (above).

An additional predicted hallmark of a stress-promoted transition is that promoted local changes occur at different positions in different cells, but with a tendency for even spacing (Kleckner et al., 2004; below). Late prophase is accompanied by formation of two such patterns. Early prometaphase chromosome axes exhibit a regular "barber pole" of alternating, evenly spaced TopoII/condensin hyper-abundant domains (Maeshima and Laemmli, 2003; Ono et al., 2003) that must have developed at late prophase. Additionally, as sister axes split, they develop inter-axis bridges, which also tend to be evenly spaced (data not shown). Analogously, stress-promoted patterning at early prophase could explain even spacing of mid-prophase axis kinks.

The above patterns are all consistent with the idea that chromosome morphogenesis from early prophase to metaphase involves alternating periods in which (1) energy (stress) is stored within the chromosomes via compaction and installation of tethering linkages, and (2) critical transitions are driven by release of that previously stored energy, with accompanying relief of stress.

Implications

We previously suggested that the chromosomal program throughout the cell cycle would comprise global chromosome compaction/expansion stress cycles (Kleckner et al., 2004). This possibility is supported here by identification of such cycles during a period previously envisioned to comprise smooth compaction. In toto, the following sequence is possible. Very compact anaphase chromosomes expand into telophase, providing stress-promoted development of new G1 chromosome organization (Gibcus and Dekker, 2013), which is locked by compaction at that stage. Chromosomes expand into S phase, with evenly spaced replication origin firings (Lebofsky et al., 2006), and then compact into G2, setting the stage for onset of morphogenesis. The early prophase-to-metaphase expansion/compaction cycles then ensue. Finally, we observe jumping apart of sisters at pre-anaphase (our unpublished data), consistent with an expansion phase, prior to compaction at anaphase, thus completing the cell cycle.

Stress-promoted processes will confer two intrinsic advantages. First, release of accumulated stress will provide discrete local progression from an existing state to the desired new state. Second, because chromosomes are coherent mechanical objects over significant length scales (Almagro et al., 2004; Pope et al., 2006; Zidovska et al., 2013), a change in stress at one position will automatically tend to redistribute outward, in one, two, or three dimensions, dissipating with distance. Such effects can create self-limiting spatial domains. Moreover, as multiple events occur sequentially, they will fill in the holes between previous events and thus tend to be evenly spaced (Kleckner et al., 2004; Zhang et al., 2014a, 2014b).

Additional advantages accrue because expansion promotes separation of chromatin segments or units. Such separation can promote release of previously established linkages (e.g., in autocatalytic bursts; Figure 7C). Expansion can also serve as a stringency factor. By providing an energetic barrier to establishment of new linkages, it can ensure that such links occur preferentially between the (appropriate) most favorable positions, rather than between all of many molecularly possible positions. For example, as loops form along a chromosome, extension/distension will disfavor formation of "too-small" loops while at the same time disfavoring formation of loops between very far-away segments on the same or on other chromosomes (e.g., in a "persistence length hypothesis"; Zickler and Kleckner, 1999).

Finally, by the stress hypothesis, molecules of already known function will be implicated in accumulation, sensing, transducing, and/or releasing chromosome expansion stress. Structural molecules (e.g., cohesins, condensins, and CTCF) have roles in organizing/constraining chromatin throughout the cell cycle (e.g., Tedeschi et al., 2013; Gibcus and Dekker, 2013; Ono et al., 2013). HEAT repeat proteins are important components of chromosomes and can serve as spring-like stress sensors (Kumar et al., 2014; Grinthal et al., 2010). TopoII will also be critical. Compact conditions will bias TopoII-mediated duplex/duplex passages toward introduction of topological linkages; more expanded conditions will bias the reaction toward elimination of topological linkages. Thus, TopoII could play unanticipated modulatory roles throughout the cell cycle (e.g., Figure 7C). Moreover, because all molecular and topological tethers will be in mechanical linkage, diverse functional interactions can be expected independent of direct physical associations among the players.

We anticipate that our results, coupled with this conceptual framework, will stimulate a new way of thinking about chromosomal states, transitions, and the roles of molecules during the eukaryotic cell cycle.

EXPERIMENTAL PROCEDURES

Additional details are provided in the Supplemental Experimental Procedures.

Cell Lines

Human HeLa and HeLa histone H2B-GFP cell lines, pig LLC-Pk EGFP-TopoIIα cell line, and Indian Muntjac cell line DM87 were gifts of J. Shah, D. Lleres, G. Gorbsky, and P. Cook, respectively.

Cell Culture and Synchronization

Cells were grown in Dulbecco's minimum essential medium (Life Technologies) with 10% (v/v) fetal bovine serum (FBS). For living cell time-lapse,

cells were synchronized at the G2/prophase boundary by incubation with 9 μM CDK1 inhibitor RO3306 (Calbiochem) for 20 hr (Vassilev et al., 2006). Cells enter prophase within 1 hr after release. For most snapshot studies, cells were synchronized at the G1/S boundary by hydroxyurea (Sigma-Aldrich; 2 mM for 20 hr). Cells reach prophase ~6 hr after release. For Figures 4B, 4E, S2, and S6, HeLa cells were synchronized by double thymidine block.

Immunofluorescence

Whole Cells

Cells were rinsed in phosphate-buffered saline (137 mM NaCl, 10 mM phosphate, 2.7 mM KCl, pH 7.4, PBS) and fixed with 100% methanol at −20°C for 20 min. For Figures 4B and 4C–4E, a "pre-extraction" method was used to differentially remove loosely bound proteins. Cells were rinsed in either 0.1% Triton X-100 in HMK buffer (20 mM HEPES, pH 7.5, 1 mM $MgCl_2$, 100 mM KCl) or XBE2 (10 mM HEPES, pH 7.7, 2 mM $MgCl_2$, 100 mM KCl, and 5 mM EGTA before fixation in methanol or 2% paraformaldehyde). Following fixation, cells were rinsed with PBS, permeabilized with 0.1% (v/v) Triton X-100 in PBS (PBST), and incubated in 5% BSA in PBST for 2 hr. Cells were incubated with the primary antibodies overnight at 4°C, washed in PBST three times, incubated for 1 hr at room temperature with secondary antibodies, washed in PBST, and stained with 1 μg/ml 4',6-diamidino-2-phenylindole (DAPI) in PBS before mounting with ProLong Gold anti-fade reagent (Life Technologies).

Primary antibodies: monoclonal mouse anti-TopoIIα (Millipore) at 1:300; polyclonal rabbit anti-Rad21 at 1:400 (gift of Dr. José Luis Barbero, Spain); polyclonal rabbit anti-hCAPH2 at 1:500 (gift of Dr. Tatsuya Hirano, Japan); and polyclonal rabbit anti-Lamin B1 at 1:600 (Abcam). Secondary antibodies (all at 1:800 dilution): donkey anti-rabbit IgG Alexa fluor 488 and 594 and donkey anti-mouse IgG Alexa fluor 488, 555, and 594 (Life Technologies).

Chromosome Spreads

Synchronized cells were collected after trypsinization, suspended in hypotonic buffer of 50% culture medium in water for 6 min, fixed in freshly made 3:1 methanol-acetic acids, and air-dried on slides. For Figures 5F and S6, harvested cells were rinsed in MES wash (1 M sorbitol, 0.1 M MES, 1 mM EDTA, 0.5 mM $MgCl_2$, pH 6.5), lysed, spread on a slide with 1% Lipsol (LIP), and fixed by 2% w/v paraformaldehyde.

Imaging

Fixed whole cells and spreads were visualized on an Axioplan IEmot microscope (Zeiss) or inverted Nikon-Ti microscope (Nikon) using appropriate filters. Images were collected using MetaMorph (Molecular Devices) image acquisition. Images in Figure 4 were subjected to 1× deconvolution.

Live-Cell Imaging and Image Processing

Cells were cultured on poly-lysine-coated glass-bottom dishes (MatTek) in CO_2-independent medium without phenol red (Life Technologies) with 10% FBS. ICRF-193 drug (Sigma-Aldrich) was added at 2 μg/ml immediately prior to observation. LLC-Pk EGFP-TopoIIα cells were observed on an inverted Zeiss LSM780 scanning confocal microscope with a temperature control at 37°C. A complete z stack with a step size of 0.2 μm (40 images per stack) was collected every 5 min using Zen software. HeLa H2B-EGFP cells were observed on an inverted Nikon-Ti microscope with a temperature control at 30°C. A complete z stack with a step size of 0.1 μm (50–60 images per stack) was collected every 2 min using a home-made MATLAB code (F.S.C. and N.K., unpublished data) or MetaMorph (Molecular Devices). For DNA staining of living cells, cells were incubated in DMEM with 0.1 μg/ml Hoechst 33342 for 5–10 min prior to observation. All images are deconvolved 1× unless otherwise noted, using AutoQuant (Media Cybernetics, Inc.) with appropriate point spread functions (Fisher et al., 2013).

Differential Sister-Chromatid Staining

Unsynchronized muntjac cells growing on coverslips were incubated in growth medium with 8 μg/ml 5-bromo-2′-deoxyuridine (BrdU, Life Technologies) for 44 hr. Cells were fixed in −20°C methanol and air-dried. Samples were stained by 5 μg/ml Hoechst 33342 for 10 min at room temperature, rinsed thoroughly, and exposed to sunlight for 30 min in a moist condition. Samples were observed in the inverted Nikon-Ti microscope.

Image Analysis

Position co-alignment in two fluorescence channels was implemented using 0.5 μm diameter multi-color beads (Invitrogen T7284). Beads were dried onto a slide, and images taken in DAPI, FITC, and Cy3 channels were co-aligned using ImageJ to define discrepancies between channels. The appropriate correction (always one pixel or less) was applied to experimental images. Volume, length, and width analyses used Volocity (PerkinElmer) and ImageJ (NIH) software. Three-dimensional reconstructions (Figures 4A and 5L) were made by PyMOL (Fisher et al., 2013).

SUPPLEMENTAL INFORMATION

Supplemental Information includes Supplemental Experimental Procedures and seven figures and can be found with this article online at http://dx.doi.org/10.1016/j.cell.2015.04.030.

ACKNOWLEDGMENTS

The authors thank T. Hirano, P.R. Cook, H. Kimura, J.L. Barbero, and G. Gorbsky for reagents, Kleckner laboratory members for helpful discussions, and B. Weiner and J. Henle for help with manuscript preparation. Work was supported by a grant to N.K. (NIH-RO1-GM025326).

Received: January 4, 2015
Revised: March 20, 2015
Accepted: April 9, 2015
Published: May 21, 2015

REFERENCES

Almagro, S., Riveline, D., Hirano, T., Houchmandzadeh, B., and Dimitrov, S. (2004). The mitotic chromosome is an assembly of rigid elastic axes organized by structural maintenance of chromosomes (SMC) proteins and surrounded by a soft chromatin envelope. J. Biol. Chem. *279*, 5118–5126.

Bajer, A. (1959). Changes in length and volume of mitotic chromosomes in living cells. Hereditas *45*, 579–596.

Deming, P.B., Cistulli, C.A., Zhao, H., Graves, P.R., Piwnica-Worms, H., Paules, R.S., Downes, C.S., and Kaufmann, W.K. (2001). The human decatenation checkpoint. Proc. Natl. Acad. Sci. USA *98*, 12044–12049.

Fisher, J.K., Bourniquel, A., Witz, G., Weiner, B., Prentiss, M., and Kleckner, N. (2013). Four-dimensional imaging of E. coli nucleoid organization and dynamics in living cells. Cell *153*, 882–895.

Gibcus, J.H., and Dekker, J. (2013). The hierarchy of the 3D genome. Mol. Cell *49*, 773–782.

Giménez-Abián, J.F., Clarke, D.J., Mullinger, A.M., Downes, C.S., and Johnson, R.T. (1995). A postprophase topoisomerase II-dependent chromatid core separation step in the formation of metaphase chromosomes. J. Cell Biol. *131*, 7–17.

Grinthal, A., Adamovic, I., Weiner, B., Karplus, M., and Kleckner, N. (2010). PR65, the HEAT-repeat scaffold of phosphatase PP2A, is an elastic connector that links force and catalysis. Proc. Natl. Acad. Sci. USA *107*, 2467–2472.

Hirota, T., Gerlich, D., Koch, B., Ellenberg, J., and Peters, J.M. (2004). Distinct functions of condensin I and II in mitotic chromosome assembly. J. Cell Sci. *117*, 6435–6445.

Kawamura, R., Pope, L.H., Christensen, M.O., Sun, M., Terekhova, K., Boege, F., Mielke, C., Andersen, A.H., and Marko, J.F. (2010). Mitotic chromosomes are constrained by topoisomerase II-sensitive DNA entanglements. J. Cell Biol. *188*, 653–663.

Kireeva, N., Lakonishok, M., Kireev, I., Hirano, T., and Belmont, A.S. (2004). Visualization of early chromosome condensation: a hierarchical folding, axial glue model of chromosome structure. J. Cell Biol. *166*, 775–785.

Kleckner, N. (2006). Chiasma formation: chromatin/axis interplay and the role(s) of the synaptonemal complex. Chromosoma *115*, 175–194.

Kleckner, N., Zickler, D., and Witz, G. (2013). Molecular biology. Chromosome capture brings it all together. Science *342*, 940–941.

Kleckner, N., Zickler, D., Jones, G.H., Dekker, J., Padmore, R., Henle, J., and Hutchinson, J. (2004). A mechanical basis for chromosome function. Proc. Natl. Acad. Sci. USA *101*, 12592–12597.

Kumar, A., Mazzanti, M., Mistrik, M., Kosar, M., Beznoussenko, G.V., Mironov, A.A., Garrè, M., Parazzoli, D., Shivashankar, G.V., Scita, G., et al. (2014). ATR mediates a checkpoint at the nuclear envelope in response to mechanical stress. Cell *158*, 633–646.

Kuwada, Y. (1939). Chromosome structure. A critical review. Cytologia (Tokyo) *10*, 213–256.

Lebofsky, R., Heilig, R., Sonnleitner, M., Weissenbach, J., and Bensimon, A. (2006). DNA replication origin interference increases the spacing between initiation events in human cells. Mol. Biol. Cell *17*, 5337–5345.

Losada, A., Hirano, M., and Hirano, T. (2002). Cohesin release is required for sister chromatid resolution, but not for condensin-mediated compaction, at the onset of mitosis. Genes Dev. *16*, 3004–3016.

Ma, K., and Shi, L.M. (1988). [Comparative studies on synaptonemal complexes in spermatocytes of Chinese muntjac *Muntiacus reevesi*, black muntjac *M. crinifrons* and Indian muntjac *M. muntjak*.]. Yi Chuan Xue Bao *15*, 282–289.

Maeshima, K., and Laemmli, U.K. (2003). A two-step scaffolding model for mitotic chromosome assembly. Dev. Cell *4*, 467–480.

Maeshima, K., and Eltsov, M. (2008). Packaging the genome: the structure of mitotic chromosomes. J. Biochem. *143*, 145–153.

Marsden, M.P., and Laemmli, U.K. (1979). Metaphase chromosome structure: evidence for a radial loop model. Cell *17*, 849–858.

Møens, P.B., and Pearlman, R.E. (1988). Chromatin organization at meiosis. BioEssays *9*, 151–153.

Moens, P.B., and Earnshaw, W.C. (1989). Anti-topoisomerase II recognizes meiotic chromosome cores. Chromosoma *98*, 317–322.

Naumova, N., Imakaev, M., Fudenberg, G., Zhan, Y., Lajoie, B.R., Mirny, L.A., and Dekker, J. (2013). Organization of the mitotic chromosome. Science *342*, 948–953.

Nakajima, M., Kumada, K., Hatakeyama, K., Noda, T., Peters, J.-M., and Hirota, T. (2007). The complete removal of cohesin from chromosome arms depends on separase. J. Cell Sci. *120*, 4188–4196.

Ohnuki, Y. (1968). Structure of chromosomes. I. Morphological studies of the spiral structure of human somatic chromosomes. Chromosoma *25*, 402–428.

Ono, T., Fang, Y., Spector, D.L., and Hirano, T. (2004). Spatial and temporal regulation of Condensins I and II in mitotic chromosome assembly in human cells. Mol. Biol. Cell *15*, 3296–3308.

Ono, T., Losada, A., Hirano, M., Myers, M.P., Neuwald, A.F., and Hirano, T. (2003). Differential contributions of condensin I and condensin II to mitotic chromosome architecture in vertebrate cells. Cell *115*, 109–121.

Ono, T., Yamashita, D., and Hirano, T. (2013). Condensin II initiates sister chromatid resolution during S phase. J. Cell Biol. *200*, 429–441.

Page, S.L., and Hawley, R.S. (2004). The genetics and molecular biology of the synaptonemal complex. Annu. Rev. Cell Dev. Biol. *20*, 525–558.

Peters, J.-M., and Nishiyama, T. (2012). Sister chromatid cohesion. Cold Spring Harb. Perspect. Biol. *4*, 4.

Pope, L.H., Xiong, C., and Marko, J.F. (2006). Proteolysis of mitotic chromosomes induces gradual and anisotropic decondensation correlated with a reduction of elastic modulus and structural sensitivity to rarely cutting restriction enzymes. Mol. Biol. Cell *17*, 104–113.

Tavormina, P.A., Côme, M.-G., Hudson, J.R., Mo, Y.-Y., Beck, W.T., and Gorbsky, G.J. (2002). Rapid exchange of mammalian topoisomerase II α at kinetochores and chromosome arms in mitosis. J. Cell Biol. *158*, 23–29.

Tedeschi, A., Wutz, G., Huet, S., Jaritz, M., Wuensche, A., Schirghuber, E., Davidson, I.F., Tang, W., Cisneros, D.A., Bhaskara, V., et al. (2013). Wapl is an essential regulator of chromatin structure and chromosome segregation. Nature *501*, 564–568.

Vassilev, L.T., Tovar, C., Chen, S., Knezevic, D., Zhao, X., Sun, H., Heimbrook, D.C., and Chen, L. (2006). Selective small-molecule inhibitor reveals critical mitotic functions of human CDK1. Proc. Natl. Acad. Sci. USA *103*, 10660–10665.

Zhang, L., Espagne, E., de Muyt, A., Zickler, D., and Kleckner, N.E. (2014a). Interference-mediated synaptonemal complex formation with embedded crossover designation. Proc. Natl. Acad. Sci. USA *111*, E5059–E5068.

Zhang, L., Wang, S., Yin, S., Hong, S., Kim, K.P., and Kleckner, N. (2014b). Topoisomerase II mediates meiotic crossover interference. Nature *511*, 551–556.

Zickler, D., and Kleckner, N. (1999). Meiotic chromosomes: integrating structure and function. Annu. Rev. Genet. *33*, 603–754.

Zidovska, A., Weitz, D.A., and Mitchison, T.J. (2013). Micron-scale coherence in interphase chromatin dynamics. Proc. Natl. Acad. Sci. USA *110*, 15555–15560.